CAMBRIDGE
UNIVERSITY PRESS

Article

Ermakovite (NH₄)(As₂O₃)₂Br, a new exhalative arsenite bromide mineral from the Fan-Yagnob coal deposit, Tajikistan

Vladimir Yu. Karpenko[1], Leonid A. Pautov[1,2], Oleg I. Siidra[3,4]* (iD), Mirak A. Mirakov[1], Anatoly N. Zaitsev[5],

Pavel Yu. Plechov[1] and Saimudasir Makhmadsharif[6]

[1]Fersman Mineralogical Museum, Russian Academy of Sciences, Leninskiy pr. 18-2, 119071 Moscow, Russia; [2]Institute of Mineralogy of South Urals Federal Research Center of Mineralogy and Geoecology UB RAS, Miass, Chelyabinsk district, 456317, Russia; [3]Department of Crystallography, St. Petersburg State University, University Emb., 7/9, St. Petersburg, 119034, Russia; [4]Kola Science Center, Russian Academy of Sciences, Apatity, Murmansk Region, 184200 Russia, 683006, Russia; [5]Department of Mineralogy, St. Petersburg State University, University Emb., 7/9, St. Petersburg, 119034, Russia; and [6]Institute of Geology, Earthquake Engineering and Seismology, Academy of Sciences of the Republic of Tajikistan, Aini 267, 734063, Dushanbe, Tajikistan

Abstract

In terrestrial rocks, Br minerals are extremely rare with only nine minerals known where Br is a dominant component. A new arsenite bromide mineral ermakovite, (NH₄)(As₂O₃)₂Br, was discovered at the tract of Kukhi-Malik, Fan-Yagnob coal deposit, ca. 75 km N of Dushanbe, Tajikistan. Ermakovite is a fumarolic mineral formed directly from gas from a natural underground coal fire. Associated minerals are sulfur, realgar, amorphous As-sulfides, salammoniac, alacránite, bonazziite and thermessaite-(NH₄). In addition, there are amorphous As₂S₃ intergrowths associated with ermakovite. The mineral typically occurs as tabular or prismatic hexagonal crystals up to 200 μm with the following forms: c (001), m (010) and p (014). Spherulites and multi-twinned intergrowths are very common. The mineral is optically uniaxial (–), $\omega = 1.960$ (5) and $\varepsilon = 1.716(3)$ (589 nm). The measured density is 3.64(2) g/cm³. The mineral is insoluble in water, HCl, HNO₃ and organic solvents. The empirical formula calculated on the basis of (As+Sb) = 4 atoms per formula unit is [(NH₄)₀.₉₂Na₀.₀₁]₀.₉₃(As₃.₉₄Sb₀.₀₆)₄.₀₀O₆.₀₂(Br₀.₉₇Cl₀.₀₈I₀.₀₁)₁.₀₆. The strongest lines in the powder X-ray diffraction pattern are [d, Å (I, %) (hkl)]: 9.160 (80)(001); 4.560(90)(002); 3.228(100) (102); 2.629(80)(110); and 2.522(60)(103). Ermakovite is hexagonal, $P6/mmm$, $a = 5.271(3)$, $c = 9.157(6)$ Å, $V = 220.3(3)$ Å³ and $Z = 1$. The sandwich-type structure of ermakovite is based on three types of layers: (1) a honeycomb [As₂O₃] arsenite layer; (2) an NH₄⁺ layer; and (3) a Br layer. The layer stacking sequence is ⋯NH₄–As₂O₃–Br–As₂O₃–NH₄⋯. Ermakovite has a synthetic analogue. Infrared and Raman spectra are also reported.

An overview of the processes that give rise to high concentrations of Br, leading to the formation of exotic Br minerals, is given.

Introduction

Br is a rare but important element in the geochemistry of cosmic rocks, terrestrial rocks and the hydrosphere (Vernadsky, 1934; Correns, 1956; Harlov and Aranovich, 2018). Due to strong incompatibility, the Br content is extremely low in mantle rocks (5.1–22 ppb, Jagoutz *et al.*, 1979) and increases in continental crust, with an average concentration of 2.5 ppm (Vinogradov, 1962; Krauskopf, 1979). Among igneous rocks, the highest content of Br is observed in alkaline rocks (e.g. haüynophyres, bergalites and phonolites from the Kaiserstuhl Complex, which contain up to 33.5 ppm Br, Wang *et al.*, 2014) and carbonatites, particularly in alkali-rich gregoryite–nyerereite carbonatites from the Oldoinyo Lengai volcano (up to 100 ppm, Mangler *et al.*, 2014). Sodalite-group minerals seem to be a major host for Br in alkaline rocks (e.g. 76 ppm Br in sodalite from the syenite of the Tamazeght alkaline-carbonatite complex, Wang *et al.*, 2016).

Much less Br is present in halogen-rich amphibole-, mica- and apatite-group minerals (Marks *et al.*, 2012; Wang *et al.*, 2016).

High Br content is observed in sedimentary rocks, particularly in evaporates (50–200 ppm) and marine sediments (up to 100 ppm) (Correns, 1956; Kendrick, 2016, 2018; Worden, 2018). Seawater, meteoric water and formation waters in sedimentary basins are also important reservoirs for the halogens (Kendrick, 2018; Worden, 2018). Evaporation of seawater, which contains 66 ppm Br on average, in sedimentary basins can lead to the formation of residual Br-rich solution or bittern and crystallisation of Br-bearing minerals, e.g. halite, sylvinite and carnallite (Kurnakov *et al.*, 1936; Fontes and Matray, 1993; Li *et al.*, 2015). Seawater is also home for various marine plants and microorganisms that contain significant amounts of Br, e.g. seaweed (kelp) with 1000–2000 ppm and plankton with 1000–4000 ppm (Correns, 1956; Kendrick, 2018).

In terrestrial rocks, Br minerals *sensu stricto* are extremely rare (Mi and Pan, 2018). Bromine is a minor constituent in several dozen minerals, where it partially replaces Cl and I. Only nine minerals are known where Br is a dominant component in at least one symmetrically independent crystallographic site (IMA mineral list, January 2022, Pasero, 2022). Almost all of these form in oxidation zones of various hydrothermal multi-commodity

deposits: barlowite, $Cu_4FBr(OH)$; bromargyrite, $AgBr$; eddavidite, $Cu_{12}Pb_2O_{15}Br_2$; grechishchevite, $Hg_3S_2BrCl_{0.5}I_{0.5}$; kadyrelite, Hg_4Br_2O; kuzminite, Hg_2Br_2; kelyanite, $(Hg_2)_6SbBrCl_2O_6$; and vasilyevite, $(Hg_2)_{10}O_6I_3Br_2Cl(CO_3)$. Only one Br mineral, demicheleite-Br, $BiSBr$, has been described from volcanic fumaroles of the La Fossa crater, Volcano island, Italy. The latter is an example of a high Br enrichment in active volcanic systems, where the element is fixed in minerals deposited from fumarolic gases, e.g. salammoniac, $(NH_4)Cl$, with 2.0–15.2 wt.% Br (Coradossi *et al.*, 1996). High Br content was identified in salammoniac (Bernard, 1985) and sylvite (Africano *et al.*, 2002) formed as the incrustations in silica tubes installed in volcanic fumaroles.

The new Br mineral ermakovite, $(NH_4)(As_2O_3)_2Br$, (IMA2020-054, Karpenko *et al.*, 2020, symbol Ekv) was found in sublimates in highly altered coal occurring in the upper reaches of the Kukhi-Malik tract, at the Fan-Yagnob coking coal deposit (Ermakov, 1935) in the Aini district of the Sogdiiskaya region, Central Tajikistan. The coals in this area are enriched in various metals (Fozilov and Alidodov, 2017).

However, the Br contents in the Fan-Yagnob coal is unknown and available data for coal from different worldwide occurrences show highly variable Br content from 0.1 to 1620 ppm (e.g. Vassilev *et al.* 2000a, 2000b; Spears 2005; Peng and Wu 2014). A very high Br content, up to 6900 ppm, was determined from coals at the Beringen mine, Belgium (Block and Dams, 1975). The element may occur in different coal components including organic matter (apparently a major host for Br), crystalline and amorphous inorganic constituents and porous solution/fluid (Eskenazy and Vassilev, 2001). Burning of coal, e.g. in thermoelectric power stations, results in the formation of different Br-enriched combustion products including solid waste material (bottom and fly ashes), flue-gas desulfurisation residues and waste water and ~90% (up to 97% in laboratory studies) of original Br in coal could be released into the atmosphere (e.g. Vassilev *et al.*, 2000b; Sajwan *et al.*, 2006; Peng and Wu, 2015).

This paper describes the occurrence, physical properties, composition and crystal structure of ermakovite with an origin related to the natural burning of coal. The new mineral is named for Nikolai P. Ermakov (1913–1993), Professor of Mineralogy, head of the thermobarogeochemistry lab and founder of the Earth Science Museum at Moscow State University, Russia. N.P. Ermakov was a participant of the famous Tajik-Pamir expedition in 1933–1934. He was engaged in initial studies of the origin of the underground coal fires at the Fan-Yagnob coal deposit that he called "*the factory of minerals*" (Ermakov, 1935).

Occurrence and paragenesis

Kukhi-Malik natural coal fires and origin of the mineral

At Kukhi-Malik (also known as Kukh-i-Malek or Kukh-i-Molik) (39°12′25″N, 68°33′59″E), the ermakovite occurs in sublimations from the gases related to a natural extensive underground coal fire of a non-anthropogenic origin known since ca. 1000 BCE. One of the early descriptions of the fires was done by Pliny the Elder (the first century AD): "*Flagrat in Bactris Cophanti noctibus vertex*" (The summit of Cophant burns in Bactris by night) (Plini the Elder, 1866). To date, the coal fire is distributed over an area of ~0.04 km^2 at the top of Kan-Tag Mountain, on the right bank of the Yagnob River (Fig. 1a,b). The geology of the Fan-Yagnob deposit and the origin of the fires have been described in several publications (Ermakov, 1935; Novikov and Suprychev, 1986).

Spontaneous combustion of the coal initiated by self-ignition is considered to be the main cause. More than 40 mineral species have been described in Kukhi-Malik sublimations to date. Several new anhydrous sulfate minerals were reported recently from this occurrence (e.g. Pautov *et al.*, 2020) and the crystallisation conditions are still insufficiently understood. Sublimates of both active and extinct underground coal fires have been known since ancient times as sources of salammoniac, sulfur, alum and saltpetre. Gas vents ('fumaroles') are very abundant at Kukhi-Malik. The temperature of gases varies widely in the range 40–590°C (Novikov *et al.*, 1979) and ermakovite crystallises in the temperature range 250–320°C. There are ~40 minerals described to date in sublimations from this area (e.g. Ermakov, 1935; Nasdala and Pekov, 1993; Mirakov *et al.*, 2019; Pautov *et al.*, 2020).

Associated minerals

Ermakovite was found in sublimates near the Big Grotto 'fumarole'. This series of fumaroles is located along a fissure in altered argillites (Fig. 1b–d). Well-crystallised mineral crusts of yellow, orange–yellow and carmine-red colours have a thickness of 1 to 5 mm and mainly consist of sulfur, realgar, salammoniac, bonazziite, alacránite, thermessaite-(NH_4), undetermined Al-sulfates and amorphous As-sulfides (Karpenko *et al.*, 2021). Ermakovite (Fig. 2) usually forms overgrowths on realgar and bonazziite and is associated closely with amorphous yellow As_2S_3. Intergrowths of the latter are distributed zonally in ermakovite crystals (Fig. 2g, h).

Appearance, physical and optical properties

Ermakovite typically occurs as tabular or prismatic hexagonal crystals up to 200 μm in maximum dimension (Fig. 2d–f). The following forms were measured using a ZRG-3 goniometer: c (001), m (010) and p (014). Spherulites and multi-twinned intergrowths are very common (Fig. 2a–c). The colour of ermakovite is yellow. Many of the individual crystals are zoned with a transparent yellowish core and semi-transparent yellow rim formed due to the admixture of amorphous As sulfides (Fig. 2h). The streak is white with a yellowish tint. The lustre is sub-adamantine. Ermakovite is very brittle and individual plates are elastic. Cleavage is perfect on (001). The fracture is uneven. Hardness is 1–1½ (VHN = 40 kg·mm^{-2} (38–46 kg·mm^{-2} at 20 g load). A standard set of immersion liquids was used to measure ε, and a solution of white phosphorus and methylene iodide with sulfur ('West liquid') was used to measure ω. Ermakovite is optically uniaxial (–), ω = 1.960(5) and ε = 1.716(3) (589 nm). The mineral is non-pleochroic under the microscope. The density measured by flotation in Clerici solution is 3.64(2) g·cm^{-3}. The density calculated based on the empirical formula of the holotype is 3.747 g·cm^{-3}. The Gladstone–Dale compatibility index, $1 - (K_p/K_c) = 0.016$, is superior.

The mineral is insoluble in water, HCl, HNO_3 and organic solvents (ethanol, iodine methylene, acetone and benzol). In Clerici liquid, a black rim is soon formed after the immersion of the mineral into liquid. The latter is the reason for the difference between the observed and calculated density values.

Infrared and Raman spectroscopy

In order to obtain an infrared (IR) absorption spectrum (Fig. 3a), a powdered sample of ermakovite was mixed with dried KBr, pelletised, and analysed using a 75-IR spectrometer. The IR
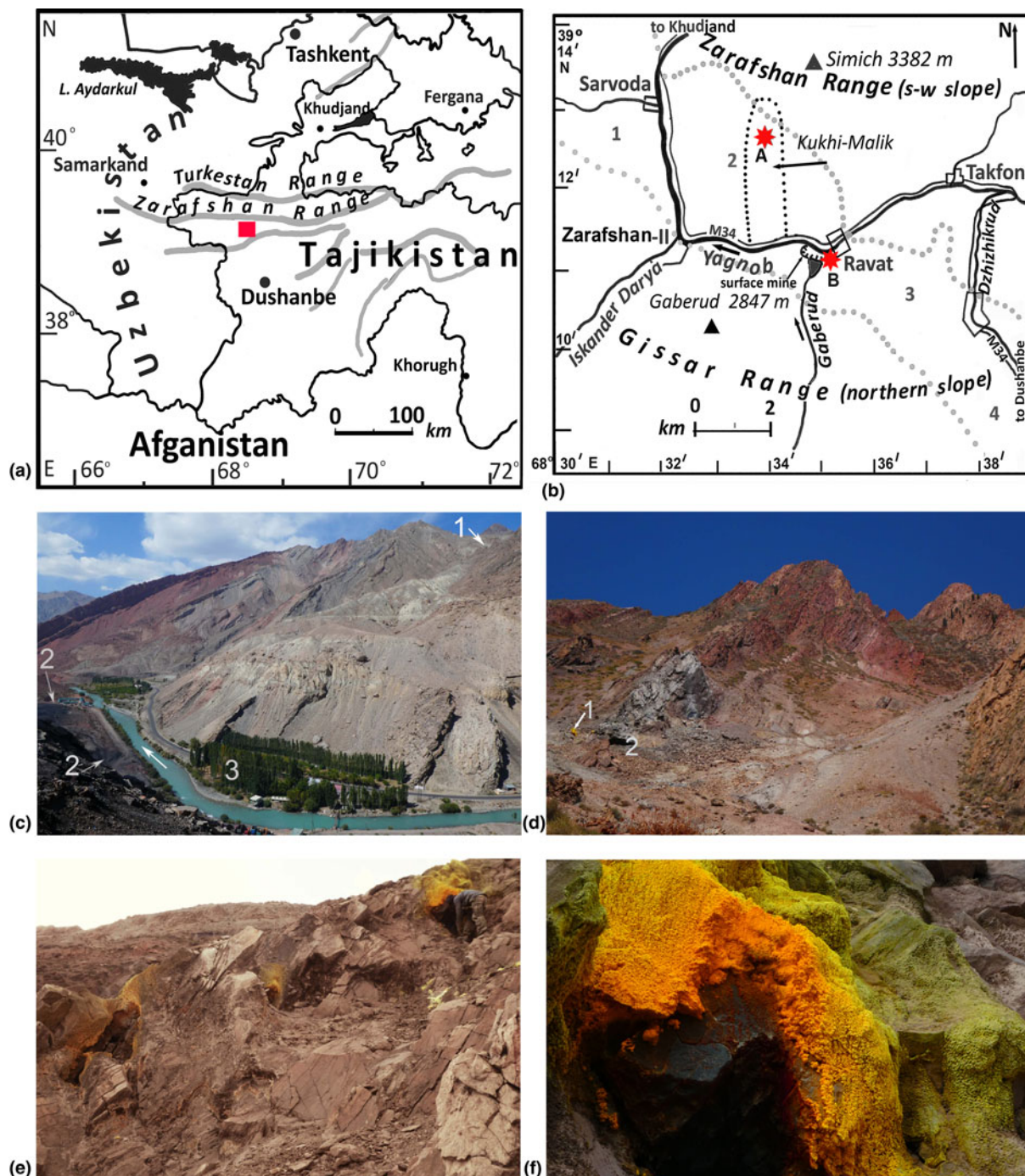
Fig. 1. Geographical map showing the location (a red rectangle) of the Fan-Yagnob coal deposit (a). A detailed contour-map of the deposit (b). Type locality of ermakovite is shown by ✴A and Ravat kishlak (village) is shown by ✴B. Grey dots mark boundaries of the deposit. 1- Eastern part of the deposit, 2–4 Central part of the deposit: 2 - Kukhi-Malik, 3-Ravat, 4-Dzhizhikrud. A general view of the area from the bank of the Yagnob River (c) (1 - Kukhi-Malik tract with underground coal fires; 2 – lower section of the Fan-Yagnob coal deposit, 3 – Ravat village (white arrow on the river designates the direction of flow). The upper reaches of the Kukhi-Malik tract (d): 1 – gas vents with the rich As–S exhalative mineralisation, where ermakovite was found; 2 - 'Big Grotto' gas vent. Three gas vents are located along the fissure in the altered argillites (Big Grotto is at the top right) (e). Enlarged view of Big Grotto with As–S mineral crusts of yellow, orange–yellow and carmine-red colours (f).

spectrum of an analogous pellet of pure KBr was used as a reference. Obtained spectra demonstrate ammonium bands at 1400–1425 cm^{-1}. The bands in the region 550–700 cm^{-1} correspond to As–O stretching vibrations of the $(AsO_3)^{3-}$ group.

Raman spectra were obtained on polished ermakovite samples using a DXR2xi Thermo Scientific Raman Imaging Microscope in the range of 3400 cm^{-1} to 70 cm^{-1} using 1 cm^{-1} resolution, 25 μm pinhole aperture, grating of 1800 lines/mm and scan time of 0.13 s with 15 scans. The excitation source was a laser with a wavelength of 532 nm at 100% power at the sample (10 mW). The spectra were recorded at room temperature. Obtained spectra and Raman maps were processed using Thermo Scientific *OMNIC* software.
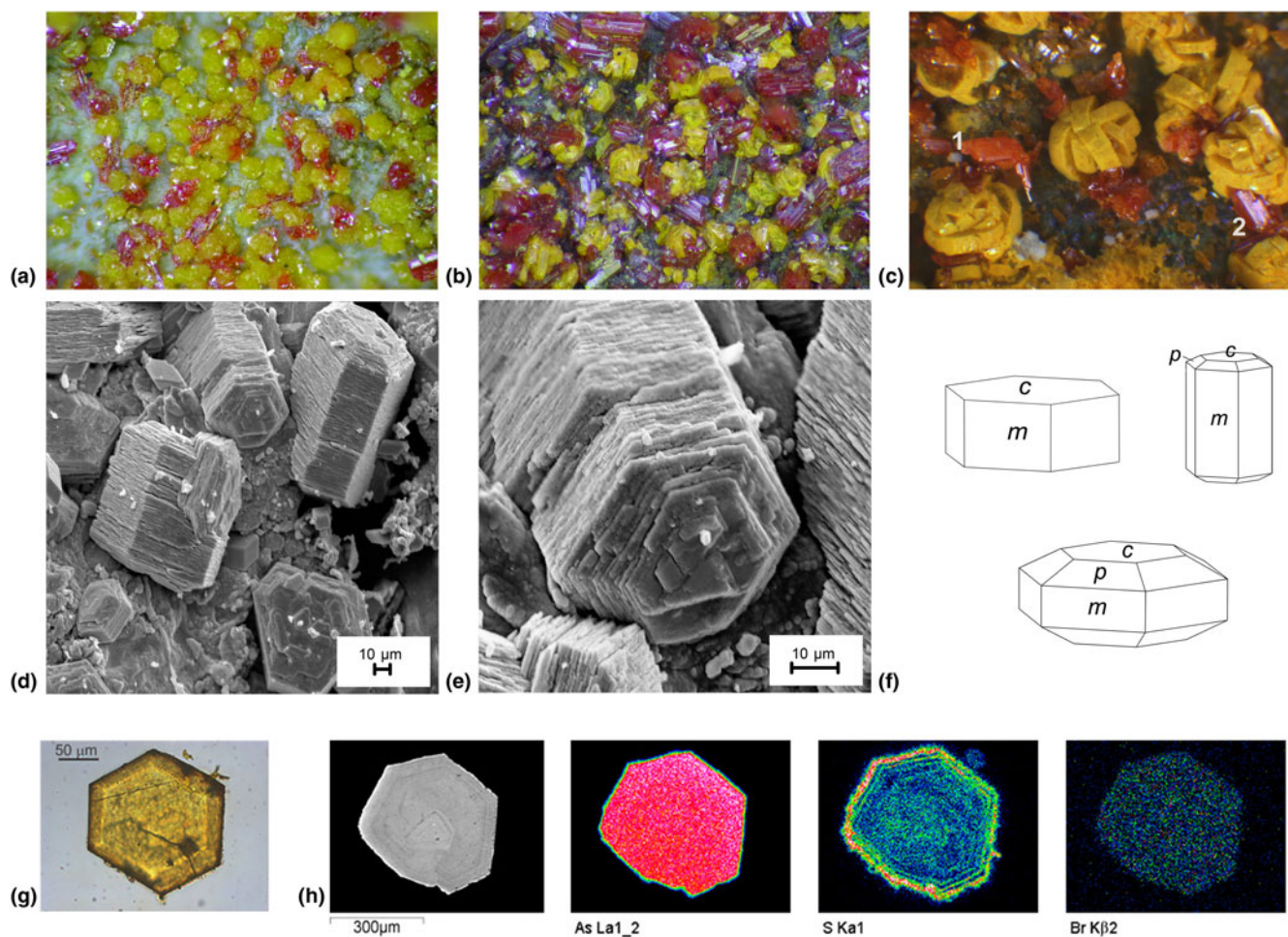
Fig. 2. Yellow ermakovite with red realgar and orange-red bonazziite (FOV 5 mm in (a) and FOV 1 mm in (b)). Multiple twins of ermakovite closely associating with bonazziite (1) and realgar (2) (FOV 2 mm) (c). Ermakovite crystals of prismatic and tabular habit. SEM images (d,e) and ideal crystal drawings (f). Thin section of zoned ermakovite crystal (g) and colour-coded X-ray element distribution maps (h). The sulfur-enriched zone is represented by the admixture of amorphous As_2S_3.

Raman spectra of ermakovite are shown in Fig. 3b. In general, the region from 1000 to 50 cm^{-1} is similar to those of the previously described natural and synthetic representatives of the MAs(III)$_4$O$_6X$ [M = (NH$_4$), K and Na; X = Cl, Br and I] family (Kampf *et al.*, 2020). Bands at 677 and 539 cm^{-1} can be assigned as As–O stretching and bending vibrations, respectively (Szymanski *et al.*, 1968; Bahfenne and Frost, 2010; Kampf *et al.*, 2020). In the range 320–400 cm^{-1}, Raman spectra of ermakovite exhibit a shoulder due to an impurity of amorphous As_2S_3, which has a strong band at 338 cm^{-1} (Fig. 3b). Raman maps were done for several ranges (690–660, 580–530, 360–330 and 190–160 cm^{-1}) to characterise the distribution of amorphous As_2S_3 throughout ermakovite crystals (Fig. 4). A band at 3176 cm^{-1} corresponds to the H–N stretching of the ammonium group.

Chemistry

Crystals of ermakovite were mounted in epoxy resin and polished with MetaDi diamond suspension (Buehler). The composition of ermakovite was studied using a CamScan 4D scanning electron microscope equipped with an Oxford Instruments INCA Energy Dispersive Spectrometer (EDS) and JCXA-733 (JEOL) analyser with a Si–(Li) detector with ATW2 ultrathin window

and INCA Energy 350 analysis system (20 kV accelerating voltage, 1 nA electron beam current measured with a Faraday cup and a beam of 25 μm were used for the analysis). BN (N$K\alpha$), InAs (As$K\alpha$), CuSbS$_2$ (Sb$L\alpha$), CuBr (freshly prepared) (Br$K\alpha$), HgCl (Cl$K\alpha$), CuI (I$L\alpha$), jadeite USNM (Na$K\alpha$), SiO$_2$ (O$K\alpha$) and BaSO$_4$ (S$K\alpha$) were used as standards. Because ermakovite contains volatile components, the EDS analysis is preferable to wavelength dispersive spectroscopy (WDS). The EDS spectra of ermakovite in the range 0.1–3.3 keV (Supplementary Fig. S1) and WDS spectra of N$K\alpha$ in ermakovite are compared with boron nitride (Supplementary Fig. S2) to demonstrate that the analytical lines do not overlap. The crystals of ermakovite are zoned (Fig. 2 and Fig. 4) with respect to the distribution of sulfur. The central parts of the crystals also reveal heterogeneity in sulfur in the range from 0.24 to 1.78 wt.%. Sulfur is not a minor component of ermakovite and corresponds to the amorphous As_2S_3 admixture. The average amount of As_2S_3 admixture from five analyses is 2.02 wt.%. Note that amorphous As_2S_3 is well-known from coal dump fires at the Kateřina mine, Czech Republic (Sejkora, 2002; Bonazzi *et al.*, 2003) and exhalative mineral assemblages at La Fossa crater, Volcano, Italy (Garavelli *et al.*, 2013).

For this reason, sulfur and arsenic content, corresponding to As_2S_3 stoichiometry, was subtracted and resulted totals
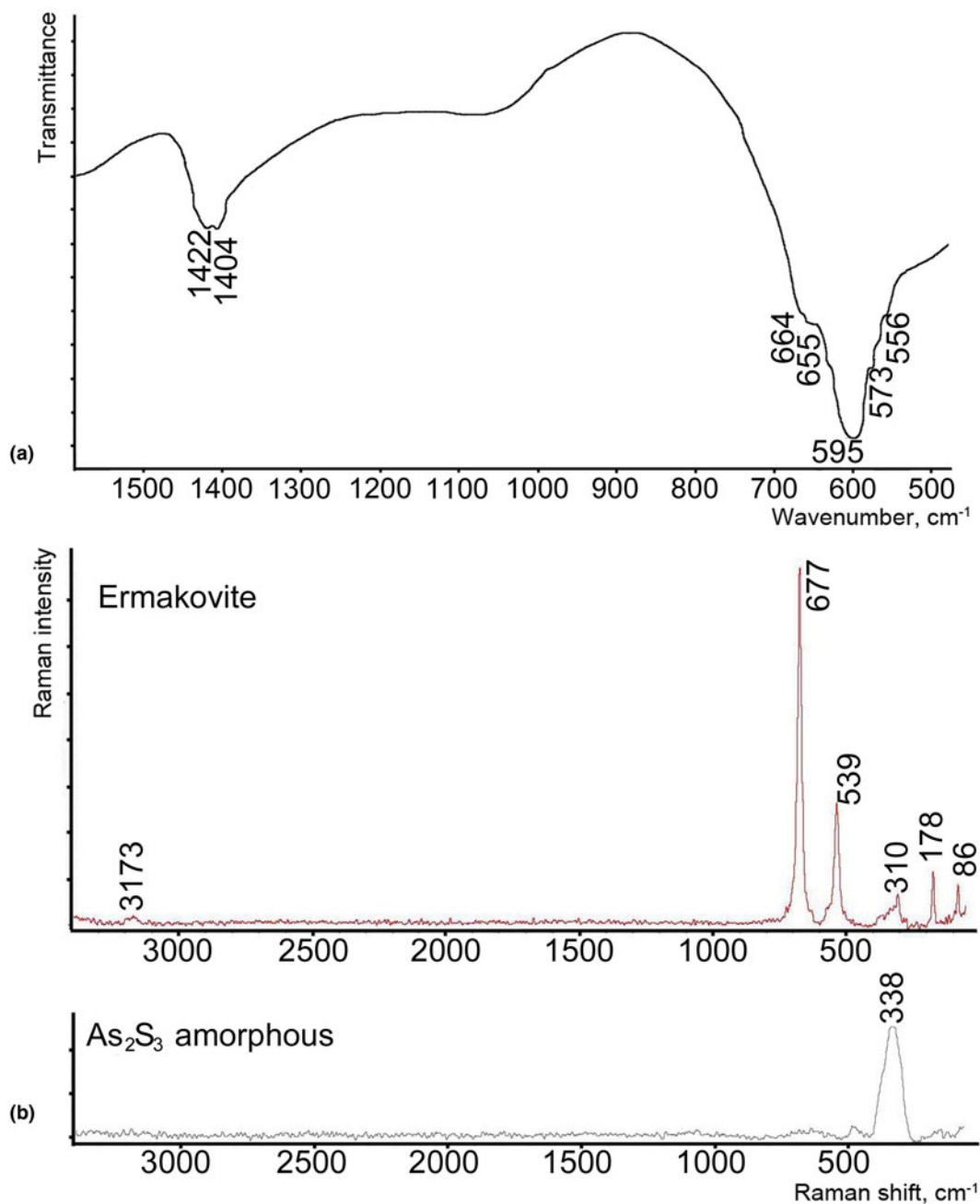
Fig. 3. Infrared (a) and Raman (b) spectra of ermakovite and synthetic amorphous As$_2$S$_3$ (c).

normalised to 100%. The results of both initial electron microprobe analysis (EMPA) data and those obtained after the subtraction are given in Table 1. The empirical formula calculated on the basis of (As+Sb) = 4 atoms per formula unit is $((NH_4)_{0.92}Na_{0.01})_{0.93}(As_{3.94}Sb_{0.06})_{4.00}O_{6.02}(Br_{0.97}Cl_{0.08}I_{0.01})_{1.06}$. The simplified formula is $(NH_4)(As_2O_3)_2Br$. Antimony (up to 2.35 wt.% Sb) partially replaces arsenic in ermakovite. Considerable amounts of Sb (13.1–17.3 wt.%) has been determined in the arsenite torrecillasite, $Na(As,Sb)_4O_6Cl$ by Kampf et al. (2014).

The ammonium content in ermakovite was confirmed by the Raman and infrared spectra (Fig. 3) and by the presence of the N$K\alpha$ peak in EDS and WDS spectra (Supplementary Fig. S1).

The N$K\alpha$ peak does not overlap with other peaks and was used for the quantitative analysis.

Crystallography

Powder X-ray diffraction data were collected using Fe$K\alpha$ radiation with a Mn-filter in a RKU–86 camera; Ge was used as an internal standard. The results (in Å for Fe$K\alpha$) are given in Table 2. Unit-cell parameters refined from the powder data are as follows: hexagonal, $a = 5.257(1)$, $c = 9.139(4)$ Å and $V = 218.7(1)$ Å^3.

A crystal of ermakovite (Table 3) was mounted on a thin glass fibre for X-ray diffraction analysis using a Bruker APEX II DUO X-ray diffractometer with a Mo-IμS microfocus X-ray tube (λ =
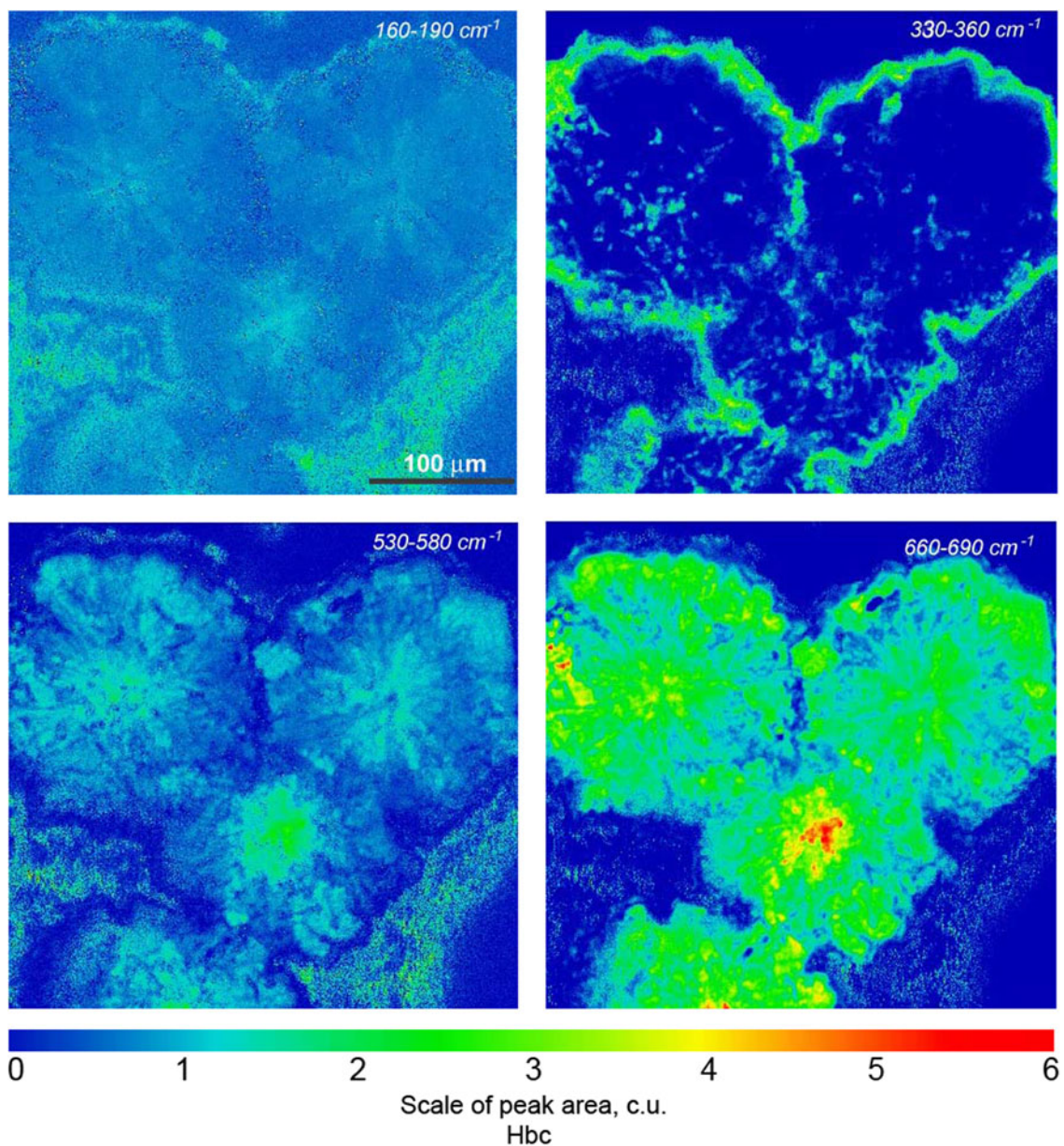
Fig. 4. Raman maps of ermakovite polished samples. The peak ranges selected for Raman mapping are labelled.

Table 1. Chemical data (in wt.%) for ermakovite.

Constituent	1		2		3		4		5		Average	
	I	II	I	II	I	II	I	II	I	II	I	II
N	2.85	2.95	2.32	2.39	2.50	2.59	2.70	2.76	2.18	2.30	2.51	2.60
H(calc.)	0.82	0.85	0.67	0.69	0.72	0.75	0.78	0.79	0.63	0.66	0.72	0.75
Na	–	–	0.17	0.17	–	–	–	–	–	–	0.03	0.03
As	59.04	60.34	59.00	59.63	57.87	58.60	58.14	58.95	59.02	59.26	58.61	59.36
Sb	1.05	1.09	1.66	1.71	2.27	2.35	1.31	1.34	0.86	0.91	1.43	1.48
Br	14.37	14.88	15.03	15.45	15.07	15.61	15.43	15.75	15.34	16.18	15.05	15.57
Cl	0.58	0.60	0.62	0.64	0.58	0.60	0.6	0.61	0.49	0.52	0.57	0.59
I	0.42	0.43	0.20	0.21	0.26	0.27	–	–	0.31	0.33	0.24	0.25
O	18.21	18.86	18.59	19.11	18.56	19.23	19.41	19.81	18.83	19.86	18.72	19.37
S	0.48	0.00	0.63	–	0.82	–	0.24	–	1.78	0.00	0.79	–
Total	97.82	100.00	98.89	100.00	98.65	100.00	98.61	100.00	99.44	100.00	98.68	100.00

Note: 1–5 are local microprobe data (Jeol Superprobe 733); I – initial data; II – normalised data after the extraction of sulfur; 6 – average for 1–5. '–' = not detected.

Table 2. Powder X-ray diffraction data (*d* in Å) for ermakovite (br = broad). The seven strongest lines are given in bold.

I_{obs}	d_{obs} (Å)	I_{calc}	d_{calc} (Å)	*hkl*
80	**9.160**	**44**	**9.157**	**001**
90	**4.560**	**40**	**4.579**	**002**
25	4.030	4	4.085	101
100	**3.228**	**100**	**3.232**	**102**
5	3.033	2	3.052	003
80	**2.629**	**61**	**2.636**	**110**
60	**2.522**	**18**	**2.537**	**103**
		23	2.533	111
40	2.276	4	2.289	004
		11	2.284	112
		1	2.282	200
5	2.162	0.1	2.215	201
30	2.031	0.2	2.046	104
		8	2.043	202
30	1.995	14	1.995	113
40	**1.817**	**3**	**1.831**	**005**
		18	1.828	203
30	1.725	8	1.728	114
30	1.716	2	1.725	210
40br	**1.608**	**0.1**	**1.616**	**204**
		18	1.615	212
40	1.516	0.6	1.526	006
		10	1.522	300
10	1.498	18	1.504	115
		7	1.502	213
		4	1.501	301
5	1.312	10	1.318	220

0.71073 Å) operated at 50 kV and 0.6 mA at the Department of Crystallography, St. Petersburg State University. More than a hemisphere of three-dimensional XRD data was collected with frame widths of 0.5° in ω, and a 50 s count time for each frame. Then the collected data were integrated and corrected for absorption using a multi-scan type of model using Bruker software. The structure of ermakovite was solved by direct methods in *P*3 space group. The obtained structure was transformed into space group *P*6/*mmm* by the use of the *ADDSYM* algorithm incorporated into the program *PLATON*. No H sites of the ammonium cation were located. The NH$_4$ tetrahedral cation is probably rotationally disordered. A similar problem was reported recently for mauriziodiniite (Kampf *et al.*, 2020) where the published refinement of the NH$_4$:Na ratio also showed similar problems for the determination of the NH$_4$:K ratio. Consequently, the N site was assigned an occupancy of N$_{0.99}$Na$_{0.01}$ (Table 4), more consistent with the EPMA. Arsenic and Br sites, having very minor admixtures, were also assigned occupancies closer to EPMA data. Fractional atom coordinates and atomic displacement parameters are listed in Tables 4,5. Selected interatomic distances are given in Table 6. The crystallographic information files have been deposited with the Principal Editor of *Mineralogical Magazine* and are available as Supplementary material (see below).

The structure of ermakovite is isotypic with the one reported previously for synthetic (NH$_4$)(As$_2$O$_3$)$_2$Br (Pertlik, 1988). The crystal structure (Table 4, Fig. 5) contains one symmetrically independent As site, one Br site, one N site and one O site. The sandwich-type structure of ermakovite is based on three types of layers: (1) a honeycomb [As$_2$O$_3$] arsenite layer; (2) an NH$_4^+$ layer; and (3) a Br layer. The layer stacking sequence is ···NH$_4$–As$_2$O$_3$–Br–As$_2$O$_3$–NH$_4$···.

Table 3. Crystallographic data and refinement parameters for ermakovite.

Crystal data	
Space group	*P*6/*mmm*
Unit cell dimensions *a, c* (Å)	5.271(3), 9.157(6)
Unit-cell volume (Å^3)	220.3(3)
Z	1
Absorption coefficient (mm^{-1})	19.559
Crystal size (mm)	0.03×0.03×0.06
Data collection	
Temperature (K)	293
Radiation, wavelength (Å)	Mo*Kα*, 0.71073
F(000)	222
θ range (°)	2.224–25.345
h, k, l ranges	$-5 \leq h \leq 6$, $-6 \leq k \leq 5$, $-10 \leq l \leq 7$
Total reflections collected	1903
Unique reflections (R_{int})	115 (0.0995)
Unique reflections $F > 4\sigma(F)$	96
Structure refinement	
Refinement method	Full-matrix least-squares on F^2
Weighting coefficients *a, b*	0.059800, 0.0
Data/restraints/parameters	115/0/14
R_1 [$F > 4\sigma(F)$], wR_2 [$F > 4\sigma(F)$]	0.037, 0.090
R_1 all, wR_2 all	0.048, 0.095
Gof on F^2	1.160
Largest diff. peak and hole (e$^-$ Å^{-3})	1.138, −0.661

Table 4. Coordinates and isotropic displacement parameters (Å) of atoms in ermakovite.

Atom	Occupancy	*x*	*y*	*z*	U_{eq}
As1*	As$_{0.985}$Sb$_{0.015}$	⅔	⅓	0.29688(17)	0.0171(6)
Br1*	Br$_{0.97}$Cl$_{0.02}$I$_{0.01}$	0	0	½	0.0337(10)
O1	O	½	½	0.1912(10)	0.020(2)
N1*	N$_{0.99}$Na$_{0.01}$	0	0	0	0.040(9)

*Occupancies assigned to be more consistent with the EPMA data.

Table 5. Anisotropic displacement parameters (Å) of atoms in ermakovite.

Atom	U^{11}	U^{22}	U^{33}	U^{23}	U^{13}	U^{12}
As1	0.0119(7)	0.0119(7)	0.0277(10)	0	0	0.0059(4)
Br1	0.0236(14)	0.0236(14)	0.054(2)	0	0	0.0118(7)
O1	0.017(4)	0.017(4)	0.034(5)	0	0	0.013(4)
N1	0.045(15)	0.045(15)	0.028(18)	0	0	0.023(7)

Table 6. Selected interatomic distances (Å) in ermakovite.

As1–O1	1.803(5) ×3
As1–Br1	3.5666(18) ×3
N1–O1	3.164(5) ×12

Concluding remarks

Ermakovite is a new representative of the *M*As(III)$_4$O$_6$*X* [*M* = (NH$_4$), K and Na; *X* = Cl, Br and I] family (Kampf *et al.*, 2020) (Table 7). Except for torrecillasite, minerals of this family are hexagonal with a sandwich-type structure based on [As$_2$O$_3$]$_2$ layers and originate from different geological environments. Lucabindiite (K,NH$_4$)(As$_2$O$_3$)$_2$(Cl,Br) is known from the

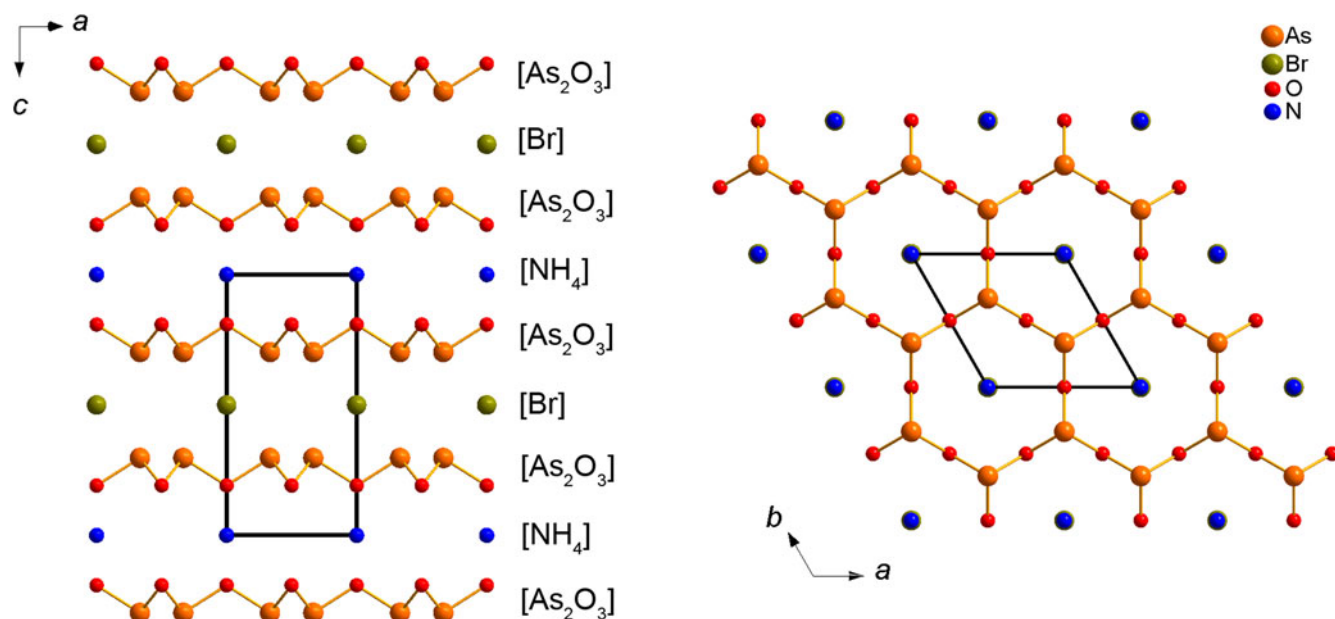**Fig. 5.** General projections of the crystal structure of ermakovite based on three types of layers: a honeycomb $[As_2O_3]$ arsenite layer; an NH_4^+ layer; and a Br layer.

Table 7. Crystallographic data for ermakovite, related minerals and synthetic compounds.

Mineral	Formula	Symmetry	Space group	a (Å)	b (Å)	c (Å)	V (Å³)	Reference
Ermakovite	$(NH_4)(As_2O_3)_2Br$	Hexagonal	$P6/mmm$	5.257(1)		9.139(4)	218.7(1)	This work
Synthetic	$(NH_4)(As_2O_3)_2Br$	Hexagonal	$P6/mmm$	5.265(1)		9.148(2)	219.6	Pertlik (1988)
Lucabindiite	$(K,NH_4)(As_2O_3)_2(Cl,Br)$	Hexagonal	$P6/mmm$	5.2386(7)		9.014(2)	214.23	Garavelli *et al.* (2013)
Mauriziodiniite	$(NH_4)(As_2O_3)_2I$	Hexagonal	$P6/mmm$	5.289(2)		9.317(2)	225.68(18)	Kampf *et al.* (2020)
Torrecillasite	$Na[(As,Sb)_2O_3]_2Cl$	Orthorhombic	$Pmcn$	5.2580(9)	8.0620(13)	18.654(3)	790.7(2)	Kampf *et al.* (2014)
Russoite	$(NH_4)ClAs_2O_3(H_2O)_{0.5}$	Hexagonal	$P622$	5.259(2)		12.590(5)	301.55(2)	Campostrini *et al.* (2019)

sublimates at the La Fossa crater, Vulcano, Aeolian Islands, Italy, whereas torrecillasite, $Na[(As,Sb)_2O_3]_2Cl$ and mauriziodiniite, $(NH_4)(As_2O_3)_2I$ were found in the oxidation zone at the Torrecillas mine, Iquique Province, Chile. Ermakovite is the first bromine dominant member of this family. A significant bromine content was previously detected in lucabindiite (3.70–10.31 Br, wt.%) (Garavelli *et al.*, 2013). A $(NH_4)(As_2O_3)_2(I,Br)$ phase was reported from the sublimates extracted from the quartz ampoules installed in the fumaroles at the Momotomba volcano, Nicaragua (Bernard, 1985), but no chemical quantitative analysis was reported. No bromine admixture was detected for mauriziodiniite and torrecillasite (Kampf *et al.*, 2016, 2020).

To date, no bromine minerals have been reported previously from the Fan-Yagnob coal deposit. No bromine has been found in salammoniac directly associated with ermakovite. Only 0.18 wt.% Br was found in some salammoniac samples found by Yu.V. Gritsenko in 2019 in gas vents located ~650 metres down the slope from the Big Grotto. The conditions for crystallisation by the means of gas transport reactions are present in a narrow range of thermochemical environments (Symonds and Reed, 1993). Similar environments yielding mineral assemblages that include various metal–halide species are observed in the fumarole fields of many volcanoes (e.g. Mutnovsky, Russia; Volcano, Italy; Merapi, Indonesia; Zelenski and Bortnikova, 2005; Demartin *et al.*, 2009, 2010; Symonds, 1993). Bromine can be accommodated in sulfide–halides of the demicheleite-type

BiS*X* (*X* = Cl, Br and I) minerals (Demartin *et al.*, 2008, 2009, 2010) or by halides of NH_4, Pb, Bi, Cd and Tl and oxyhalides of the $MAs(III)_4O_6X$-type (Coradossi *et al.*, 1996; Garavelli *et al.*, 1997, 2013). Similar processes take place in active underground coal fires. Ermakovite is the first example of an oxybromide mineral formed in such conditions, accommodating the overwhelming majority of bromine, while the neighbouring salammoniac remains nearly bromine-free.

References

Africano F., Van Rompaey G., Bernard A. and Le Guern F. (2002) Deposition of trace elements from high temperature gases of Satsuma-Iwojima volcano. *Earth, Planets and Space*, **54**, 275–286.

Bahfenne S. and Frost R.L. (2010) A review of the vibrational spectroscopic studies of arsenite, antimonite, and antimonate minerals. *Applied Spectroscopy Reviews*, **45**, 101–129.

Bernard A. (1985) *Les Mécanismes de Condensation des Gaz Volcaniques (Chimie, Minéralogie et Équilibres des Phases Condensées Majeures et Mineures)*. PhD thesis, Université Libre de Bruxelles, Belgium, 412 pp.

Block C. and Dams R. (1975) Inorganic composition of Belgian coals and coal ashes. *Environmental Science and Technology*, **9**, 146–150.

Bonazzi P., Bindi L., Olmi F. and Menchetti S. (2003) How many alacranites do exist? A structural study of non-stoichiometric As_8S_{9-x} crystals. *European Journal of Mineralogy*, **15**, 282–288.

Campostrini I., Demartin, F. and Scavini M. (2019) Russoite, $NH_4ClAs_2^{3+}O_3(H_2O)_{0.5}$, a new phylloarsenite mineral from Solfatara Di Pozzuoli, Napoli, Italy. *Mineralogical Magazine*, **83**, 89–94.

Coradossi N., Garavelli A., Salamida M. and Vurro F. (1996) Evolution of Br/Cl ratios in fumarolic salammoniac from Vulcano (Aeolian Islands, Italy). *Bulletin of Volcanology*, **58**, 310–316.

Correns C.W. (1956) The geochemistry of the halogens. *Physics and Chemistry of the Earth*, Volume **1**, 181–233.

Demartin F., Gramaccioli C.M., Campostrini I. and Orlandi P. (2008) Demicheleite, BiSBr, a new mineral from La Fossa crater, Vulcano, Aeolian Islands, Italy. *American Mineralogist*, **93**, 1603–1607.

Demartin F., Gramaccioli C.M. and Campostrini I. (2009) Demicheleite-(Cl), BiSCl, a new mineral from La Fossa Crater, Vulcano, Aeolian Islands, Italy. *American Mineralogist*, **94**, 1045–1048.

Demartin F., Gramaccioli C.M. and Campostrini I. (2010) Demicheleite-(I), BiSI, a new mineral from La Fossa Crater, Vulcano, Aeolian Islands, Italy. *Mineralogical Magazine*, **74**, 141–145.

Ermakov N.P. (1935) Pasrud-Yagnobskoye coal deposit and mines of the Kan-Tag mountain. Pp. 47–66 in: *On Geology of Coal Deposits of Tajikistan*. Materials of Tajik-Pamir Expedition 1933, volume **12**, [in Russian].

Eskenazy G. and Vassilev S. (2001) Geochemistry of chlorine and bromine in Bulgarian coals. *Review of the Bulgarian Geological Society*, **62**, 37–46.

Fontes J.Ch. and Matray J.M. (1993) Geochemistry and origin of formation brines from the Paris Basin, France. 1. Brines associated with Triassic salts. *Chemical Geology*, **109**, 149–175.

Fozilov Dj.N. and Alidodov D.A. (2017) Elements of the impurities in coal coalfield background Yagnob. *News of the Academy of sciences of the Republic of Tajikistan*, **167**, 101–110 [in Russian].

Garavelli A., Laviano R. and Vurro F. (1997) Sublimate deposition from hydrothermal fluids at the Fossa crater – Vulcano, Italy. *European Journal of Mineralogy*, **9**, 423–432.

Garavelli A., Mitolo D., Pinto D., Laviano R. and Vurro F. (2013) Lucabindiite, $(K,NH_4)As_4O_6(Cl,Br)$, a new fumarole mineral from the "La Fossa" crater at Vulcano, Aeolian Islands, Italy. *American Mineralogist*, **98**, 470–477.

Harlov D.E. and Aranovich L. (editors) (2018) *The Role of Halogens in Terrestrial and Extraterrestrial Geochemical Processes. Surface, Crust, and Mantle*. Springer International Publishing AG, 1030 pp.

Jagoutz E., Palme H., Baddenhausen H., Blum K., Cendales M., Dreibus G., Spettel B., Lorenz V. and Wänke H. (1979) The abundances of major, minor and trace elements in the earth's mantle as derived from primitive ultramafic nodules. *Proceedings of the 10th Lunar and Planetary Science Conference*, Volume **2**, 2031–2050.

Kampf A., Nash B., Dini M. and Molina Donoso A.A. (2014) Torrecillasite, $NaAs_4O_6Cl$, a new mineral from the Torrecillas mine, Iquique Province, Chile: description and crystal structure. *Mineralogical Magazine*, **78**, 747–755.

Kampf A.R., Nash B.P., Dini M. and Molina Donoso A.A. (2016) Gajardoite, $KCa_{0.5}As_4^{3+}O_6Cl_2 \cdot 5H_2O$, a new mineral related to lucabindiite and torrecillasite from the Torrecillas mine, Iquique Province, Chile. *Mineralogical Magazine*, **80**, 1265–1272.

Kampf A.R., Nash B.P. and Molina Donoso A.A. (2020) Mauriziodiniite, $(NH_4)(As_2O_3)_2I$, the ammonium and iodine analogue of lucabindiite from the Torrecillas mine, Iquique, Chile. *Mineralogical Magazine*, **84**, 267–273.

Karpenko V.Y., Pautov L.A., Siidra O.I. and Mirakov M.A. (2020) Ermakovite, IMA 2020-054, in: CNMNC Newsletter 58, *Mineralogical Magazine*, **84**, https://doi.org/10.1180/mgm.2020.93

Karpenko V.Yu., Pautov L.A., Mirakov M.A., Siidra O.I., Makhmadsharif S., Shodibekov M. and Plechov P.Yu. (2021) Bonazziite and alacranite from sublimates of the natural underground coal fire at Kukhi-Malik tract, Tajikistan. *New data on minerals*, **54**, 82–93.

Kendrick M.A. (2016) Halogens. Pp. 1–5 in: *Encyclopedia of Geochemistry, Volume H* (White W.M., editor). Springer International Publishing AG.

Kendrick M.A. (2018) Halogens in seawater, marine sediments and the altered oceanic lithosphere. Pp. 591–648 in: *The Role of Halogens in Terrestrial and Extraterrestrial Geochemical Processes. Surface, Crust, and Mantle* (Harlov D.E., Aranovich L., editors). Springer International Publishing AG.

Krauskopf K.B. (1979) *Introduction to Geochemistry, 2nd edition*. McGraw-Hill, Tokyo, 617 pp.

Kurnakov N.S., Kuznetsov V.G., Dzens-Litovskiy A.I. and Ravich M.I. (1936) *Salt lakes of Crimea*. Izdatelstvo Akademii nauk SSSR, Moscow-Leningrad, 278 pp. [in Russian].

Li M.G., Yan F., Wang Z.R., Liu X.M., Fang X.M. and Li J. (2015) The origins of the Mengye potash deposits in the Lanping-Simao Basin, Yunnan Province, Western China. *Ore Geology Reviews*, **69**, 174–186.

Mangler M.F., Marks M.A.W., Zaitzev A.N., Eby G.N. and Markl G. (2014) Halogens (F, Cl and Br) at Oldoinyo Lengai volcano (Tanzania): effects of magmatic differentiation, silicate–natrocarbonatite melt separation and surface alteration of natrocarbonatite. *Chemical Geology*, **365**, 43–53.

Marks A.W.M., Wenzel T., Whitehouse M.J., Loose M., Zack T., Barth M., Worgard L., Krasz V., Eby G.N., Stosnach H. and Markl G. (2012) The volatile inventory (F, Cl, Br, S, C) of magmatic apatite: an integrated analytical approach. *Chemical Geology*, **291**, 241–255.

Mi J.-X. and Pan Y. (2018) Halogen-rich minerals: crystal chemistry and geological significances. Pp. 123–184 in: *The Role of Halogens in Terrestrial and Extraterrestrial Geochemical Processes. Surface, Crust, and Mantle* (Harlov D.E. and Aranovich L., editors). Springer International Publishing AG.

Mirakov M.A., Pautov L.A., Karpenko V.Yu., Faiziev A.R. and Makhmadsharif S. (2019) Pauflerite β-VO(SO$_4$) from sublimations of the natural underground fire at Kukhi-Malik (Ravat) tract, Fan-Yagnob coal deposit, Tajikistan. *New data on minerals*, **53**, 114–120 [in Russian].

Nasdala, L. and Pekov, I.V. (1993) Ravatite, $C_{14}H_{10}$, a new organic mineral species from Ravat, Tadzhikistan. *European Journal of Mineralogy*, **5**, 699–705.

Novikov V.P. and Suprychev V.V. (1986) Conditions of the modern mineral genesis at the underground firing coals at Fan-Yagnobskoye deposit. *Mineralogia Tadzhikistana*, **7**, 91–104 [in Russian].

Novikov V.P., Suprychev V.V. and Babayev M.A. (1979) Salammoniac from sublimates of the underground coal fire at the Ravat coal deposit (Central Tadzhikistan). *Doklady Akademii nauk Tadzhikskoyi SSR*, **12**, 687 [in Russian].

Pasero M. (2022) *The New IMA List of Minerals*. International Mineralogical Association. Commission on new minerals, nomenclature and classification (IMA-CNMNC). http://cnmnc.main.jp/

Pautov L.A., Mirakov M.A., Siidra O.I., Faiziev A.R., Nazarchuk E.V., Karpenko V.Y. and Makhmadsharif, S. (2020) Falgarite, $K_4(VO)_3(SO_4)_5$, a new mineral from sublimates of a natural underground coal fire at the tract of Kukhi-Malik, Fan-Yagnob coal deposit, Tajikistan. *Mineralogical Magazine*, **84**, 455–462.

Peng B.-X. and Wu D.-S. (2014) Distribution and content of bromine in Chinese coals. *Journal of Fuel Chemistry and Technology*, **42**, 769–773.

Peng B. and Wu D. (2015) Study on bromine release from bituminous coal during combustion. *Fuel*, **157**, 82–86.

Pertlik F. (1988) The compounds KAs_4O_6X (X= Cl, Br, I) and $NH_4As_4O_6X$ (X= Br, I): Hydrothermal syntheses and structure determinations. *Monatshefte für Chemie*, **119**, 451–456.

Plini the Elder (1866) *Secundi Naturalis historia* (edited D. Detlefsen). Vol. 1, Liber 2, Sect. 106. Berolini, Weidmannos [in Latin].

Sajwan K.S., Twardowska I., Punshon T. and Alva A.K. (editors) (2006) *Coal Combustion Byproducts and Environmental Issues*. Springer, New York, 241 pp.

Sejkora, J. (2002) *Minerální asociace hořícího odvalu dolu Kateřina v Radvanicích u Trutnova a procesy jejího vzniku*. MS, disertační práce, Přírodovědecká fakulta, Masarykova univerzita, Brno, 1–144 [in Czech].

Spears D.A. (2005) A review of chlorine and bromine in some United Kingdom coals. *International Journal of Coal Geology*, **64**, 257–265.

Symonds R. (1993) Scanning electron microscope observations of sublimates from Merapi Volcano, Indonesia. *Geochemical Journal*, **26**, 337–350.

Symonds R.B. and Reed M.H. (1993) Calculation of multicomponent chemical equilibria in gas-solid-liquid systems: calculation methods, thermochemical data and applications to studies of high-temperature volcanic gases with examples from Mount St. Helens. *American Journal of Science*, **293**, 758–864.

Szymanski H.A., Marabella L., Hoke J. and Harter J. (1968) Infrared and Raman studies of arsenic compounds. *Applied Spectroscopy*, **22**, 297–304.

Vassilev S.V., Eskenazy G.M. and Vassilev C.G. (2000a) Contents, modes of occurrence and origin of chlorine and bromine in coal. *Fuel*, **79**, 903–921.

Vassilev S.V., Eskenazy G.M. and Vassilev C.G. (2000b) Contents, modes of occurrence and behaviour of chlorine and bromine in combustion wastes from coal-fired power stations. *Fuel*, **79**, 923–937.

Vernadsky V.I. (1934) *Essays on Geochemistry*. ONTI, Gorgeolneft'izdat, Moscow, 380 pp. [in Russian].

Vinogradov A.P. (1962) Average content of chemical elements in main types of the intrusive rocks of the Earth crust. *Geokhimia*, **7**, 555–571 [in Russian].

Wang L.-X., Marks M.A.W., Keller J. and Markl G. (2014) Halogen variations in alkaline rocks from the Upper Rhine Graben (SW Germany): Insights into F, Cl and Br behavior during magmatic processes. *Chemical Geology*, **380**, 133–144.

Wang L.-X., Marks M.A.W., Wenzel T. and Markl G. (2016) Halogen-bearing minerals from the Tamazeght complex (Morocco): constraints on halogen distribution and evolution in alkaline to peralkaline magmatic systems. *The Canadian Mineralogist*, **54**, 1347–1368.

Worden R.H. (2018) Halogen elements in sedimentary systems and their evolution during diagenesis. Pp. 185–260 in: *The Role of Halogens in Terrestrial and Extraterrestrial Geochemical Processes. Surface, Crust, and Mantle* (Harlov D.E. and Aranovich L., editors). Springer International Publishing AG.

Zelenski M. and Bortnikova S. (2005) Sublimate speciation at Mutnovsky volcano, Kamchatka. *European Journal of Mineralogy*, **17**, 107–118.